

Analysis of High-Field Hall-Coefficient Behavior in Uniaxially Stressed p -GaSb[†]

R. A. Metzler and W. M. Becker

Department of Physics, Purdue University, West Lafayette, Indiana 47907

(Received 30 May 1973)

Galvanomagnetic effects have been examined in p -GaSb using uniaxial compressional stresses up to 10^{10} dyn/cm² in the temperature range 50–300°K. At liquid-nitrogen temperature, the high-field Hall coefficient shows a weak relative maximum at low stresses, but decreases monotonically with further increase in stress. The high-field behavior is analyzed in terms of stress-induced decoupling of the valence bands. The analysis also includes stress-induced splitting of the impurity states and strain-dependent deformation of the energy surfaces. Although the models used can be made to fit both the low-stress and high-stress regions, a good fit cannot be obtained over the entire stress range for a single set of parameters. Qualitative arguments are presented which indicate that the full theoretical form for the deformation of the energy surfaces as given by Pikus and Bir must be utilized to explain the data.

I. INTRODUCTION

After the initial investigation of Hall¹ on p -type Ge, very little work has been done using uniaxial stress for the study of galvanomagnetic properties in p -type semiconductors. We recently reported the results of such an investigation on p -GaSb.² In that work we examined the behavior of the Hall coefficient and mobility in the temperature range 50–300°K using uniaxial compressional stresses up to 10^{10} dyn/cm². The results were interpreted in terms of the decoupling of the valence bands and the reduction of the impurity activation energies with increasing stress. A good fit was obtained to the data using a simple two-band model with uniform separation of the band edges with stress. Also, the model utilized an impurity-level scheme suggested by Jakowetz *et al.*³ from luminescence and photoconductivity results. This level scheme assumes the presence of both monovalent and divalent impurity centers. Our analysis, based on a least-squares fit of this model to the data, indicated that only the neutral state of the divalent impurity contributes carriers to band conduction at 77°K and below. An obvious feature of the data noted in our earlier results was a strong monotonic decrease of the Hall coefficient at high stress. However, there were also indications of a weak relative maximum at low stress. This latter feature is not explainable on the basis of the previous model. Additional data which we present below give further evidence of the existence of the low-stress Hall coefficient maximum. An important clue to a more complete understanding of the band structure of p -GaSb may rest on an explanation of this particular feature of the sample behavior.

The present work considers modifications of the earlier model to predict the high-field Hall-coefficient behavior over the complete stress range. Three new models, which consider different functional variations of (i) the stress-induced deforma-

tions of the valence bands, and (ii) the strain splitting of the impurity levels, are presented. The band deformations are introduced from empirical considerations. The strain dependence of the impurity-level splitting has been considered both for a monovalent and a divalent impurity. It will be shown that the prominent features of the data can be separately explained by these modifications, but a good fit cannot be obtained over the complete stress range for a single set of parameters. Qualitative arguments are presented which indicate that the full theoretical form for the deformation of the energy surfaces, as given by Pikus and Bir,⁴ must be utilized for a correct interpretation of the data.

Earlier we had assumed two-band conduction to explain the field dependence of the Hall coefficient at zero stress. We briefly analyze the experimental results for both the Hall coefficient and transverse magnetoresistance using a simple two-band approximation to justify our previous assumption. The Hall-coefficient behavior is also shown to be consistent with warped energy surfaces.

In Sec. II we discuss the experimental procedure. The results, together with our analysis, are given in Sec. III. Appendix A outlines the procedure for extracting the transport parameters from the field dependence of the Hall coefficient. In Appendix B we give the details of the derivation of the density-of-states function obtained from the Pikus-Bir theory.

II. EXPERIMENTAL PROCEDURE

Undoped single crystals of p -GaSb used in this investigation were grown by the Czochralski technique. Samples prepared for application of stress along $\langle 111 \rangle$ were cut perpendicular to the growth axis; twinning in the ingot required cutting $\langle 100 \rangle$ oriented samples oblique to the growth axis. Hall-coefficient results using two pairs of contacts indicated that all samples were homogeneous to with-

in the precision of the measurements, over the entire stress range. Sample dimensions were typically $1 \times 1 \times 8$ mm as prepared for mounting. A uniaxial-stress apparatus based on a design by Cuevas and Fritzsche⁵ and built by Seiler⁶ was employed in the measurements. Indium solder contacts were used for attaching the four potential probes and the two current leads. Stress greater than 1×10^{10} dyn/cm² was achieved in this apparatus. Temperature stability was ensured by the direct immersion of the sample in the appropriate cryogenic liquid. The following temperature baths were used: liquid freon-14 (146 °K), liquid methane (112 °K), and liquid nitrogen (77 °K). Pumped solid nitrogen was used to obtain measurements at 53 °K. The emphasis in the data acquisition was on establishing the Hall-coefficient behavior at the highest stresses possible. Because of electrode and/or sample failure, the temperature dependence of R_H and ρ on a single sample at high stresses was not experimentally accessible.

III. RESULTS AND ANALYSIS

A. Hall-Coefficient Behavior

The field dependence of the Hall coefficient at three different temperatures is shown in Figs. 1 and 2 for [111] and [100] stresses, respectively. Figure 4 gives additional data for [111] stress at

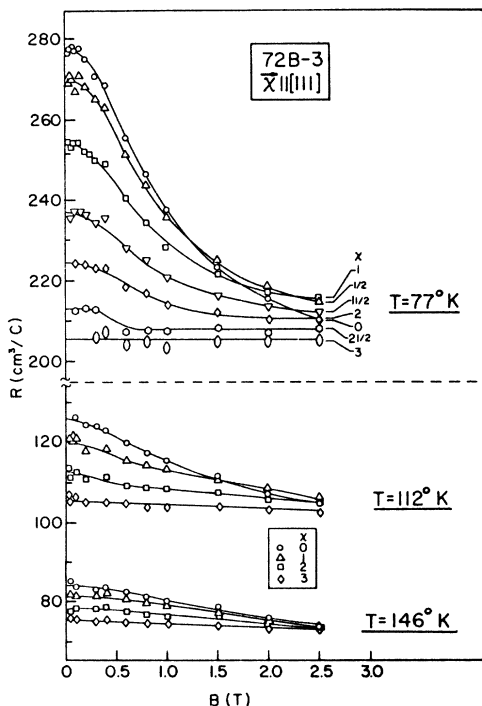


FIG. 1. Hall coefficient vs magnetic field at 77, 112, and 146 °K for $\chi \parallel [111]$. χ is in units of 10^9 dyn/cm².

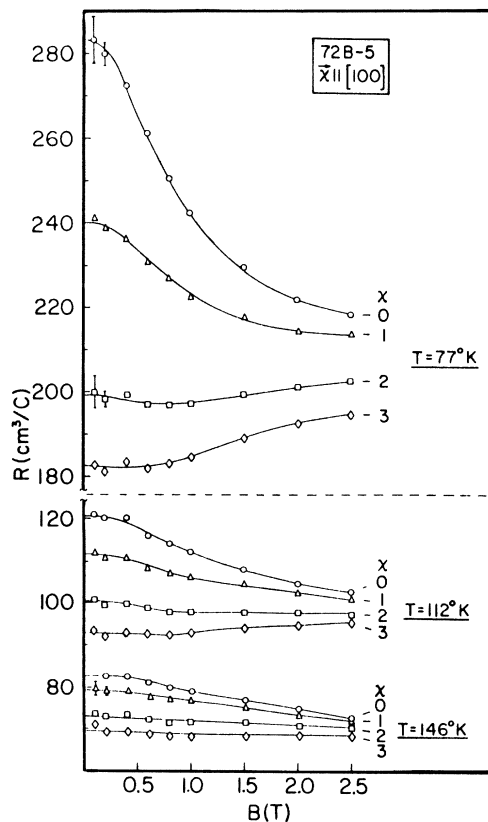


FIG. 2. Hall coefficient vs magnetic field at 77, 112, and 146 °K for $\chi \parallel [100]$. χ is in units of 10^9 dyn/cm².

53 °K. The sample behaviors are seen to be nearly independent of stress direction. At zero stress, the field dependence of R_H decreases rapidly with increasing temperature. The same effect is noted with increasing stress; as seen in both Figs. 2 and 3, the field dependence reverses noticeably at moderate stresses for both stress orientations. At $B = 0$, and at $B = 2.5$ T, R_H varies more rapidly with stress $\tilde{\chi}$ for $\tilde{\chi} \parallel [100]$ than for $\tilde{\chi} \parallel [111]$. We note a small maximum in R_H (2.5 T) versus χ for $\tilde{\chi} \parallel [111]$, as is evident in Figs. 1 and 3. Additional data, which are not presented here, confirm that the feature is also present for the case $\tilde{\chi} \parallel [100]$. This behavior, which is displayed more clearly in the inset in Fig. 4, increases in prominence at lower temperatures. In all cases except near zero stress, R_H appears to be independent of field at ~ 2.5 T. In a separate experiment, carried out at 77 °K, to 4 T, we find that at zero-stress R_H approaches saturation to within 5% at 2.5 T.

B. Magnetic Field Dependence of R_H and ρ at Zero Stress

Previous galvanomagnetic studies of *p*-GaSb utilizing uniaxial stress have been limited to a temperature region where impurity-band conduction

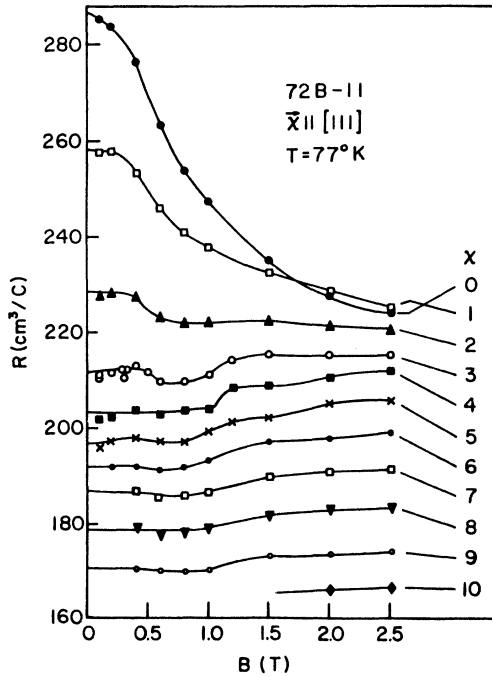


FIG. 3. Hall coefficient vs magnetic field at 77°K for $\chi \parallel [111]$. χ is in units of 10^9 dyn/cm².

dominates.⁷ Above 20°K the same results indicate normal-band conduction. Our work is in the region 50–300°K. We therefore assume an analysis based on conduction in the Γ_8 bands only.

We first treat the zero-stress Hall-coefficient data using a procedure outlined by Lavine and Ewald.⁸ The analysis is valid for conduction in two spherical parabolic bands. Later in this section we discuss a calculation which considers the ex-

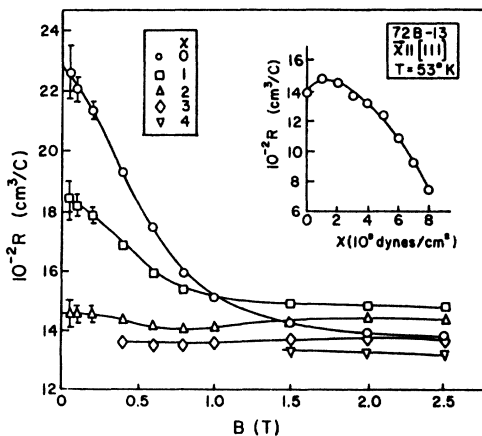


FIG. 4. Hall coefficient vs magnetic field at 53°K for $\chi \parallel [111]$. χ is in units of 10^9 dyn/cm². The inset shows the stress dependence of the Hall coefficient at $B = 2.5$ T.

pected warping of the bands.

The Lavine-Ewald procedure involves fitting the data to the following equation:

$$\frac{R_0 B^2}{\Delta R_H} = \frac{\alpha\gamma + \alpha\delta B^2}{\beta\gamma - \alpha\delta} = \frac{\gamma}{\delta} \left(\frac{R_0}{R_\infty - R_0} \right) + B^2 \left(\frac{R_0}{R_\infty - R_0} \right), \quad (1)$$

where $R_0 = R_H(B \rightarrow 0)$, $R_\infty = R_H(B \rightarrow \infty)$, and $\Delta R_H = R_H - R_0$. The quantities α , β , γ , and δ are defined in Appendix A, which outlines the details of the calculation. They are related to the transport parameters μ_l , p_l , μ_h , and p_h , where the subscripts l and h refer to the light and heavy holes, respectively. A plot of $R_0 B^2 / \Delta R_H$ versus B^2 using experimental Hall data and the zero-field conductivity σ_0 yields values of the transport parameters. Figure 5 shows a least-squares fit for sample 72B-5. The results of the fitting procedure are listed in Table I for typical samples used in the stress investigation. A similar analysis, developed by Champness⁹ for the treatment of transverse-magnetoresistance data, has also been employed. This method requires a least-squares fit to the equation

$$\rho_0 B^2 / \Delta\rho = (1 + cB^2)/b, \quad (2)$$

where ρ_0 is the zero-field resistivity, $\Delta\rho = \rho - \rho_0$, and b and c are related to the transport parameters. By assuming the approximations $\mu_l \gg \mu_h$

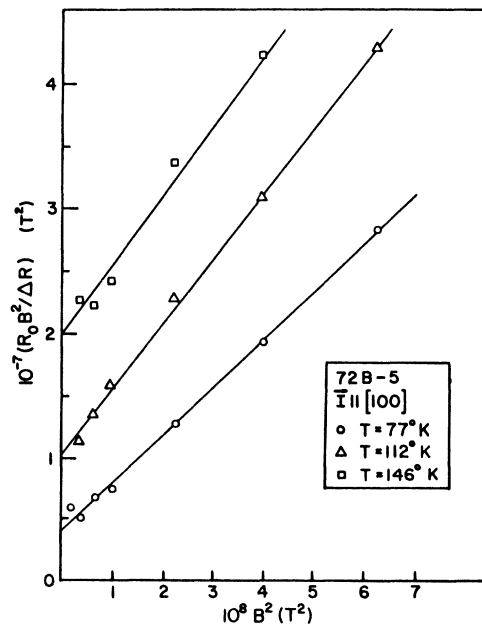


FIG. 5. Hall-coefficient dependence on magnetic field at $\chi = 0$ plotted according to Eq. (1). The straight lines represent the least-squares fit to the data.

TABLE I. Transport parameters determined from the two-band analysis of the zero-stress Hall coefficient and magnetoresistance data.

Sample	Temp. (°K)	R_0 (cm ² /C)	σ_0 [(Ω cm) ⁻¹]	p_l (cm ⁻³)	p_h (cm ⁻³)	μ_l (cm ² /V sec)	μ_h (cm ² /V sec)	Data
72B-3	77	277.5	8.91	4.74×10^{14}	3.09×10^{16}	10 800	1 600	R
				7.98×10^{14}	3.21×10^{16}	9 000	1 500	ρ
	112	125.0	15.03	8.12×10^{14}	6.20×10^{16}	8 100	1 400	R
				1.75×10^{14}	6.60×10^{16}	6 500	1 200	ρ
	146	83.0	16.89	1.52×10^{15}	8.98×10^{16}	5 200	1 100	R
				2.18×10^{15}	1.01×10^{17}	5 200	1 000	ρ
72B-5	77	280.0	8.63	4.35×10^{14}	2.96×10^{16}	10 500	1 600	R
				1.04×10^{14}	3.61×10^{16}	8 400	1 200	ρ
	112	120.0	14.55	7.64×10^{14}	6.34×10^{16}	7 600	1 300	R
				2.20×10^{15}	7.16×10^{16}	5 700	1 100	ρ
	146	82.5	16.39	1.24×10^{15}	9.12×10^{16}	5 600	1 000	R
				3.27×10^{15}	1.03×10^{17}	4 400	900	ρ

and $p_h \gg p_l$, Champness has shown that

$$\begin{aligned} \mu_l &= (c+b)/\sqrt{c}, \\ p_l &= b(\sqrt{c})\sigma_0/e(c+b)^2, \\ \mu_h &= [(c+b)/c](R_0\sigma_0 - b/\sqrt{c}), \\ p_h &= [c/(c+b)]^2(\sigma_0/e)(R_0\sigma_0 - b/\sqrt{c})^{-1}. \end{aligned} \quad (3)$$

Figure 6 shows the least-square fits obtained for sample 72B-5. The transport parameters derived from this analysis are also presented in Table I. The Hall-coefficient and resistivity results are separately designated by R and ρ in the last column of the table. Stirn and Becker¹⁰ have outlined the calculation of p_h/p_l and μ_l/μ_h for warped energy surfaces, based on an earlier method given by Lax and Mavroides¹¹ for p -Ge. We use band parameters averaged over values given by Stradling¹² and Reine *et al.*,¹³ as follows: $A=12$, $B=8$, and $C^2=144$. These give a value for $B'=9.4$, leading to $p_h/p_l=31.5$. Invoking the assumption of Stirn and Becker¹⁰ that the relaxation times for both types of holes are equal, we get $\mu_l/\mu_h=8.23$. The experimental mobility ratios obtained from Table I are seen to be close to the theoretically predicted value.¹⁴ The hole-concentration ratios determined from resistivity data are close to the predicted value, while those obtained from Hall data are no more than a factor of 2 greater than expected.

We briefly consider the complications introduced by a more realistic model, which includes warping of the hole surfaces and mixed scattering. A theoretical treatment of the field dependence of the Hall coefficient for this case was first considered by Beer and Willardson¹⁵ for p -Ge. This analysis involves a calculation of $R_H(B)/R_H(\infty)$ in terms of known band parameters and a quantity β , which weights the various scattering processes

between lattice and impurity scattering. For pure lattice scattering, $\beta=0$. An approximate fit, shown in Fig. 7, was calculated using $\beta_l=10.0$, $\beta_h=3.0$, $p_l/p_h=0.09$, $\mu_l/\mu_h=8.0$, $\alpha=0.96$, $a=0.935$, $b_3=0.141$, and $b_5=0.059$. The values of α and a chosen in this work were given by Beer and Willardson for p -Ge; b_3 and b_5 were calculated using the values of A , B , and C^2 listed above. The theoretical and experimentally obtained results are plotted in Fig. 7 in terms of a magnetic field parameter $(\gamma_h^s)^{1/2}=0.75\pi^{1/2}10^{-8}\mu_h B$. Although the

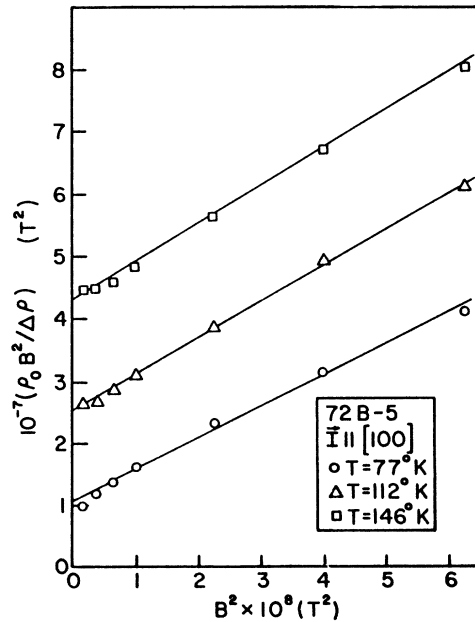


FIG. 6. Transverse magnetoresistance vs magnetic field at $\chi=0$ plotted according to Eq. (2). The straight lines represent the least-squares fit to the data.

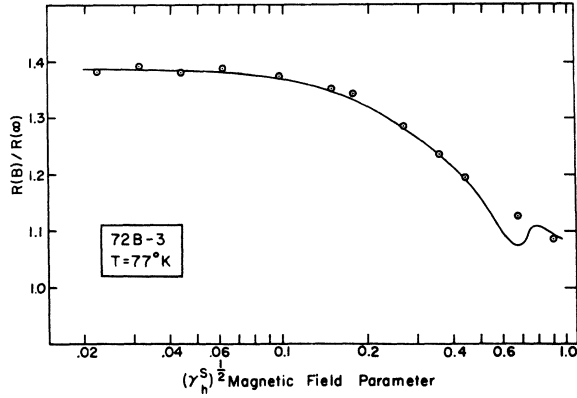


FIG. 7. Hall-coefficient dependence of magnetic field at $\chi=0$. The smooth curve is calculated from the theory of Beer and Willardson for warped surfaces. The experimental data are represented by circles.

agreement between theory and experiment appears quite good, the choice of parameters should not be considered unique. We conclude from this brief analysis that the zero-stress Hall data are consistent with warping.

Beer¹⁶ has shown that the Hall-coefficient factor $R_H(B)/R_H(\infty)$ may rise monotonically to saturation values for a single warped-band model. As pointed out previously, our stress data are interpretable in terms of decoupling of the valence bands. It is therefore possible that the rise in the Hall coefficient with field, seen in Figs. 2 and 3 at moderate stresses, may be indicative of conduction in a single warped band. An analysis of this feature awaits more detailed information regarding the deformation of the hole surfaces and changes of scattering mechanisms with stress.

C. Stress Dependence of Hall Coefficient at Strong Fields

At strong fields, the Hall factor $r \rightarrow 1$, leading to a useful simplification in the determination of the total carrier concentration. By restricting our attention to this field region, we avoid complications arising from deformation of the hole surfaces and the complexities introduced by considering energy-dependent scattering mechanisms. We assume that $R_H(2.5 \text{ T}) \approx R_H(\infty) = [e(p_i + p_h)]^{-1}$ for all stress values. Earlier we showed that the temperature dependence of $R_H(2.5 \text{ T})$ at zero stress could be fitted using a level scheme involving a single divalent impurity center. As mentioned in Sec. I, the neutral state of this impurity, which occurs at 34.5 meV, is the only level needed to account for band conduction at 77°K and below.

1. Model I

The first model which we consider assumes that the neutral state exhibits the properties of a mono-

valent impurity level under stress. Bir *et al.*¹⁷ have investigated the effects of stress on shallow monovalent acceptors in Ge and Si. For such crystals, they indicate that the levels split under uniaxial strain into two twofold-degenerate states. The splitting is described by the following relation:

$$\Delta = 2 \left\{ \frac{1}{2} b'^2 [(\epsilon_{xx} - \epsilon_{yy})^2 + (\epsilon_{xx} - \epsilon_{zz})^2 + (\epsilon_{yy} - \epsilon_{zz})^2] + d'^2 (\epsilon_{xy}^2 + \epsilon_{xz}^2 + \epsilon_{yz}^2) \right\}^{1/2}, \quad (4)$$

where b' and d' are the impurity-level deformation potentials and the ϵ_{ij} 's are components of the strain tensor. The theory is appropriate for $\Delta \ll |E_i|$, where E_i is the ionization energy of the impurity. For the two stress orientations involved in our experiments, the splittings are as follows:

$$\begin{aligned} \Delta &= (1/\sqrt{3}) d' S_{44} |\chi| \quad \text{for } \vec{\chi} \parallel [111], \\ \Delta &= 2b' (S_{11} - S_{12}) |\chi| \quad \text{for } \vec{\chi} \parallel [100], \end{aligned} \quad (5)$$

where the S_{ij} 's are the elastic compliance components and χ is the applied stress ($\chi < 0$ for compressive stress). (Since the analysis for $\vec{\chi} \parallel [100]$ is completely analogous to the results for $\vec{\chi} \parallel [111]$, we will only carry out calculations for the case of $\vec{\chi} \parallel [111]$ for which we have more extensive data.) Combining the above result with the zero-stress ionization energy E_i^0 , we can represent the splittings in the form

$$E_i^\pm = E_i^0 \pm \gamma \chi, \quad (6)$$

where γ is half the proportionality factor given in Eq. (5) for $\vec{\chi} \parallel [111]$.

According to the work of Bir and Pikus,¹⁸ when a uniaxial compressional stress is applied along a [100] or [111] crystallographic direction in a semiconductor having diamond or zinc-blende crystal structure, the degeneracy of the $J = \pm \frac{3}{2}$ state is partially removed. The fourfold-degenerate Γ_8 bands are split into two doubly degenerate states with $M_j = \pm \frac{3}{2}$ and $M_j = \pm \frac{1}{2}$. Under compressive stress the $M_j = \pm \frac{1}{2}$ states (light-hole band) move to lower hole energies; complete decoupling of the valence bands is expected at infinite strain. We had previously² assumed a linear splitting of the bands but had neglected changes in hole surface geometry. Linear splitting is retained in the present work and is given by

$$E_l = -\delta \chi, \quad E_h = \delta \chi. \quad (7)$$

(Hole energies are taken as positive; therefore $\delta < 0$ for our work.) The present work takes into account deformation of the bands by considering two different functional forms for the variation of the density of states with stress. In model I the density of states of each band is assumed to vary linearly with stress. Both the theory of Pikus and Bir⁴ and the calculations of Hensel and Feher¹⁹

give identical results for the density-of-states values at infinite strain. These theories yield energy surfaces which are ellipsoids of revolution, with the unique axis along the stress direction. These surfaces can be characterized by perpendicular, m_i^* , and parallel, m_{ii}^* , mass components. For $\vec{\chi} \parallel [111]$, the mass components are related to the band parameters by the expressions

$$m_i^{*+} = \frac{1}{2} \hbar^2 (A \mp \frac{1}{6} N)^{-1}, \quad m_{ii}^{*+} = \frac{1}{2} \hbar^2 (A \pm \frac{1}{3} N)^{-1}, \quad (8)$$

where $N = [3(C^2 + 3B^2)]^{1/2}$. In Eqs. (8) the positive superscript designates the light-hole mass and is accompanied by the upper sign in the parentheses. In all subsequent calculations to be described, we used the following values for the inverse mass parameters: $A = 13$, $B = 8.6$, and $C^2 = 16$. (The theoretical behavior of the Hall coefficient is not appreciably altered for this set of parameters as compared to the behavior found using the values given in Sec. II B.) Using these parameters, we find $m_i^*(\chi \rightarrow \infty) = 0.085 m_e$ and $m_h^*(\chi \rightarrow \infty) = 0.093 m_e$, where $m_i^* = (m_x m_{ii}^{1/2})^{2/3}$. Since these mass values are nearly equal, we employ a single limiting value for both masses, $m^* = 0.0885 m_e$. Using this value of m^* for both bands, the ratio of the rates of change of the density of states with stress b_i for the two bands can be calculated. Thus we have

$$\frac{b_h}{b_i} = \frac{m_e^{*3/2} - m_h^{*3/2}(\chi=0)}{m_e^{*3/2} - m_i^{*3/2}(\chi=0)} \approx -5, \quad (9)$$

where $m_i^*(\chi=0)$ values are taken from expressions given by Lax and Mavroides¹¹ for a warped surface. According to their work, the light- and heavy-hole masses at zero stress are related to the band parameters by the following:

$$m^{*+} = \frac{1}{2} \hbar^2 (A \pm B')^{-1}, \quad (10)$$

where the signs follow the notation of Eqs. (8) and $B' = (B^2 + \frac{1}{6} C^2)^{1/2}$. From Eq. (9) the densities of states \mathcal{D}_i can be written as

$$\mathcal{D}_i = E_i^{1/2} (D_{i,0} + \lambda \chi), \quad (11)$$

$$\mathcal{D}_h = E_h^{1/2} (D_{h,0} - 5\lambda \chi),$$

where λ is an adjustable parameter which varies the rates b_i and b_h simultaneously. The quantity $D_{i,0} = 4\pi(2m_i^*/\hbar^2)^{3/2}$, where m_i^* is the zero-stress band-edge effective mass.

The curves plotted in Fig. 8 represent the theoretical behavior for a combination of both linear splitting of the impurity states and linear changes in the band density of states. The parameter $\Delta_E (= 2\delta\chi)$ on the abscissa represents the splitting of the valence bands at $k=0$. The pairs of numbers displayed adjacent to the theoretical curves represent the reduced parameters ($\lambda/2\delta$, $\gamma/2\delta$) used in the calculation. Representing the parameters in this fashion thus allows plotting of the theoretical results in a form which is independent of the band

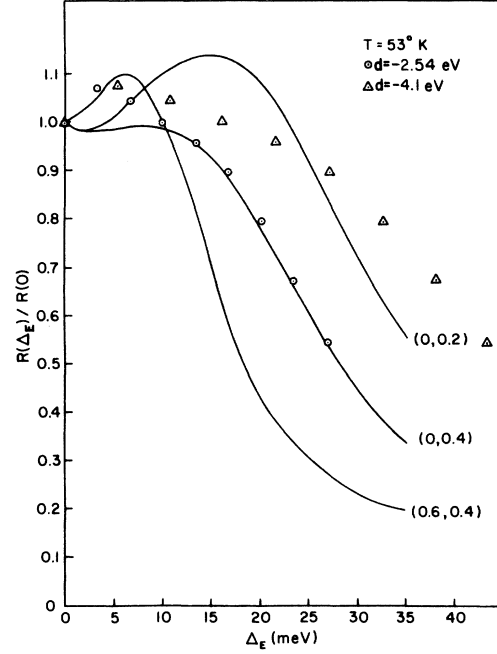


FIG. 8. Reduced Hall coefficient at 53°K vs energy separation at the band edges. The smooth curves are derived from model I.

deformation potentials and compliance coefficients. Then, by varying the deformation potential we can change the calculated value of the band splitting for a given stress, thus permitting the scaling of the experimental data to the theoretical curves. Since $\Delta_E = 2\delta\chi$, multiplication of the reduced parameters by Δ_E recovers the original variables defined in Eqs. (6) and (11). The experimental data, obtained at $B = 2.5$ T for $\vec{\chi} \parallel [111]$, are plotted for two different values of the band deformation potential d . We originally chose $d = -2.54$ eV to scale the data to the theoretical curves, whereas the choice of $d = -4.1$ eV represents an average of values reported in the literature.

As seen in the figure, maxima in R may be obtained for a constant density of states ($\lambda=0$), but these are predicted for higher stresses than are found experimentally. The inclusion of a linear variation of the density of states ($\lambda \neq 0$) shifts the maxima to lower values of Δ_E . However, it also leads to a more precipitous decrease in R at larger values of strain than is observed experimentally.

The calculations thus suggest that a better fit may be obtained by employing large density-of-states changes in the low-stress region, while deemphasizing the changes at high stresses.

2. Model II

We next consider a modification of the previous model which retains linear splitting of the impurity

states and utilizes the following density-of-states function:

$$\mathfrak{D}_i(E_i, \Delta_E) = \mathfrak{D}_i(E_i, 0) + \mathfrak{N}_i \frac{\Delta_E^2}{(a + \Delta_E)^2}, \quad (12)$$

where

$$\mathfrak{D}_i(E_i, \infty) = \mathfrak{D}_i(E_i, 0) + \mathfrak{N}_i.$$

This function embodies the gross features of the changes suggested by comparison of model I with the data. The quantity a controls the rate of change of $\mathfrak{D}_i(E_i, \Delta_E)$, and $\mathfrak{D}_i(E_i, \infty)$ represents the limiting value used in the previous model for both bands at infinite strain. Depending on the choice of the parameter a , the behavior of Eq. (12) closely approximates a density-of-states function derivable from the theory of Pikus and Bir⁴ [see Eq. (14)]. The results of the calculations based on the density-of-states function given in Eq. (12) are shown in Fig. 9. The pairs of numbers displayed adjacent to the theoretical curves represent the parameters $(a, \gamma/2\delta)$ used in the calculation. As in model I, we have used two different values of the band deformation potential d in our fitting procedure. The value $d = -3.5$ eV was chosen to represent a lower limit of the values reported in the literature. Comparison of the behavior shown in these figures with the curves corresponding to the same values of $\gamma/2\delta$ shown in Fig. 8 indicates that the nonlinear variation in the density of states provides a better fit at low stresses than was observed for a linear model, but fails in the high-stress region.

3. Model III

A recent group-theoretical investigation has been carried out by Kartheuser and Rodriguez²⁰ which gives the energy splitting of the neutral level of a divalent impurity center having Γ_6 symmetry. Their work, which considers terms linear in strain, indicates that this level splits into two nondegenerate levels and one fourfold-degenerate level. The stress dependence of these levels can be expressed as follows:

$$\begin{aligned} E_i^1 &= E_i^0 + (\alpha_1 + \gamma)\chi, \\ E_i^2 &= E_i^0 + \alpha_1\chi, \\ E_i^3 &= E_i^0 + (\alpha_1 - \gamma)\chi, \end{aligned} \quad (13)$$

where E_i^0 is the zero-stress ionization energy, α_1 determines the rate of motion with stress of the group of states as a whole, and γ controls the rate of separation of the split levels with stress. E_i^1 and E_i^3 are the nondegenerate levels. The results obtained using this model are not significantly different from those calculated for a monovalent impurity.

We noted earlier that changes in $R_H(2.5 \text{ T})$ occur more rapidly with stress for $\tilde{\chi} \parallel [100]$ than for $\tilde{\chi} \parallel [111]$. This result is predictable from the theory

of Pikus and Bir⁴ when the differences in the deformation potentials b and d are taken into consideration.

4. Theoretical Considerations

A systematic consideration of likely models leads to the examination of the behavior of the density-of-states function given by the theory of Pikus and Bir.⁴ As shown in Appendix B, for $\tilde{\chi} \parallel [111]$,

$$\mathfrak{D}_i(E_i, \Delta_E) = \frac{A_i \Delta_E^2 + B_i \Delta_E + C_i}{(D_i + F_i \Delta_E)^2}. \quad (14)$$

In this equation, the energy dependence is absorbed into the constants. Calculation of the Hall coefficient requires the numerical integration of this function, which is impractical for the current investigation. The qualitative consideration of the density-of-states function given by Eq. (14) does suggest that the theory will give a better fit to the data than the previous empirical models. Considering the variation of the average hole energy with stress, we conclude that at low stresses the theoretical density of states initially changes more rapidly than is predicted from the empirical function given by Eq. (12). At high stresses, the saturation value of the density of states for the light-hole band at the assumed average hole energy ($E \approx 10$ meV) is $\approx 2 \times 10^{15} (\text{cm}^3 \text{meV})^{-1}$. This is the same value utilized in our earlier work. (Due to the de-

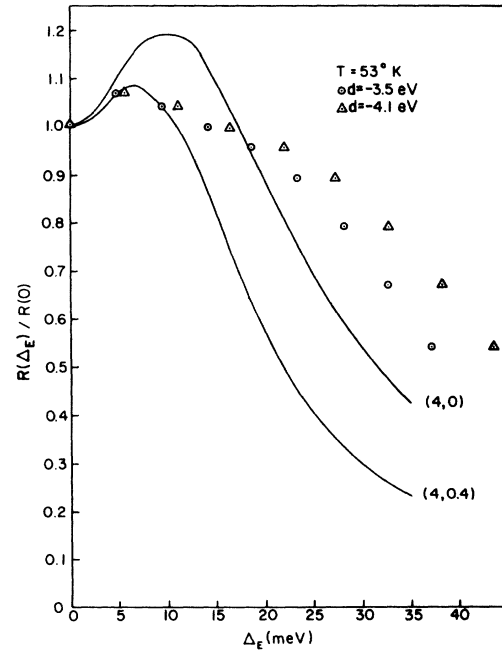


FIG. 9. Reduced Hall coefficient at 53°K vs energy separation at the band edges. The smooth curves are derived from model II.

population of carriers from the heavy-hole band with increasing stress, the effect of this band can be neglected at high stress.) It is thus reasonable to expect the theoretical behavior of the Hall coefficient using Eq. (14) to be similar to that found earlier² for the high-stress region, where a good fit was obtained. We therefore expect that the use of Eq. (14) will lead to a considerable improvement between theory and experiment.

5. Remarks

The present investigation was hindered by lack of detailed knowledge of the impurity centers in as-grown *p*-type GaSb and their behavior under stress. In this work we have presented some considerations relating to the analysis of stress-induced changes in the transport properties of this material. A definitive test of our approach should be obtainable from a similar study carried out on materials which are better characterized with respect to impurity species and concentration than in the present case. For example, Zn-doped Ge would be interesting in this respect, since the level positions and their splittings under stress have been extensively investigated both experimentally and theoretically.²¹

APPENDIX A

Assuming spherical parabolic energy surfaces, the concentrations and mobilities of both the light and heavy holes can be extracted from the dependence of the Hall coefficient on the magnetic field by fitting Eq. (1) to the experimental data. The parameters α , β , γ , and δ in this equation are defined as follows:

$$\begin{aligned}\alpha &= p_0 \mu_0^2 + p_1 \mu_1^2 = \sigma_0^2 R_0 / e, \\ \beta &= (p_0 + p_1) \mu_0^2 \mu_1^2, \\ \gamma &= (p_0 \mu_0 + p_1 \mu_1)^2 = \sigma_0^2, \\ \delta &= (p_0 + p_1)^2 \mu_0^2 \mu_1^2 = p_T^2 \mu_0^2 \mu_1^2,\end{aligned}\quad (\text{A1})$$

where σ_0 is the conductivity at $B=0$ and e is the magnitude of the charge on an electron. If we write Eq. (1) as

$$(R_0 B^2 / \Delta R_H) = I + MB^2, \quad (\text{A2})$$

we find

$$\delta = \gamma M / I = \sigma_0^2 M / I, \quad \beta = \delta e R_0 (1 + M^{-1}) = \delta / p_T, \quad (\text{A3})$$

where $p_T = p_0 + p_1$ is the total hole concentration. By determining I and M from a least-squares fit and using the experimentally determined values of R_0 and σ_0 , the parameters α , β , γ , and δ can now be found. From Eqs. (A1) we find

$$\begin{aligned}\mu_1 &= \delta^{1/2} p_T^{-1} \mu_0^{-1}, \\ p_0 &= (\mu_1 \gamma^{1/2} - \alpha) (\mu_1 \mu_0 - \mu_0^2)^{-1},\end{aligned}$$

$$\begin{aligned}p_1 &= (\mu_0 \gamma^{1/2} - \alpha) (\mu_1 \mu_0 - \mu_0^2)^{-1}, \\ \mu_0 &= \mu_1 + [(\alpha p_T - \gamma) p_0^{-1} p_1^{-1}]^{1/2}.\end{aligned}\quad (\text{A4})$$

The correct value for μ_0 is found from Eqs. (A4) by assuming an approximate initial value and using an iteration loop.

APPENDIX B

The derivation of the theoretical density-of-states function given in Eq. (14) follows a development similar to that used by Roman and Ewald.²² Starting with the dispersion relationship given by Pikus and Bir⁴ and assuming $\tilde{\chi} \parallel [100]$, we find [Eq. (A1) of Roman and Ewald]

$$\begin{aligned}E(\tilde{k}, \chi) &= E = A k^2 \pm [\alpha^2 k^4 + \delta_0 \\ &\quad + B \delta_0 (2k_{\parallel}^2 - k_{\perp}^2)]^{1/2},\end{aligned}\quad (\text{B1})$$

where

$$\alpha^2 k^4 = B^2 k^4 + C^2 (k_x^2 k_y^2 + k_x^2 k_z^2 + k_y^2 k_z^2), \quad \delta_0 = b(S_{11} - S_{12}) \chi,$$

k_{\parallel} and k_{\perp} are the components of \tilde{k} parallel and perpendicular to the stress direction, and the hydrostatic shift of the Γ_8 bands has been neglected. The upper sign refers to light holes, while the lower sign corresponds to heavy holes. This expression is now solved for k_{\parallel}^2 giving²³

$$\begin{aligned}k_{\parallel}^2 &= -k_{\perp}^2 - (\alpha^2 - A^2)^{-1} [AE + B \delta_0 \mp D_0^{1/2} [1 + 3(\alpha^2 - A^2) \\ &\quad \times B \delta_0 D_0^{-1} k_{\perp}^2]^{1/2}],\end{aligned}\quad (\text{B2})$$

where $D_0 = (A^2 - \alpha^2 + B^2) \delta_0^2 + \alpha^2 E^2 + 2ABE \delta_0$. After expanding the term under the radical, this expression can be rearranged into the form of an ellipsoid of revolution,

$$\frac{k_{\parallel}^2}{r_{\parallel}^2} + \frac{k_{\perp}^2}{r_{\perp}^2} = 1, \quad (\text{B3})$$

where $r_{\parallel}^2 = (A^2 - \alpha^2)^{-1} (AE + B \delta_0 \mp D_0^{1/2})$ and $r_{\perp}^2 = r_{\parallel}^2 \times (D_0^{1/2} \mp \frac{3}{2} B \delta_0)^{-1} D_0^{1/2}$. The volume of this constant-energy surface can now be found from $V = \frac{4}{3} \pi r_{\parallel} r_{\perp}^2$. We now make the approximation, used by Roman and Ewald, that

$$D_0 \simeq (\alpha E + B \delta_0 - \alpha \delta_0 + A \delta_0)^2. \quad (\text{B4})$$

This approximation is exact for the case of no warping ($\alpha = B$). Considering the upper signs (light holes) we find

$$V_l = \frac{4}{3} \pi \left(\frac{E_l}{A + \alpha} \right)^{3/2} \left[1 - \frac{3}{2} \frac{B}{\alpha} \left(\frac{E_l}{\delta_0} + \frac{A + B}{\alpha} \right)^{-1} \right]^{-1}, \quad (\text{B5})$$

where E_l is the energy at the edge of the light-hole band ($E_l = E - \delta_0$). For the case of heavy holes (lower signs) we make the approximation

$$D_0 \simeq (\alpha E - B \delta_0 + \alpha \delta_0 + A \delta_0)^2, \quad (\text{B6})$$

which yields

$$V_h = \frac{4}{3} \pi \left(\frac{E_h}{A - \alpha} \right)^{3/2} \left[1 + \frac{3}{2} \frac{B}{\alpha} \left(\frac{E_h}{\delta_0} + \frac{A - B}{\alpha} \right)^{-1} \right]^{-1}, \quad (\text{B7})$$

where E_h is the energy at the edge of the heavy-hole band ($E_h = E + \delta_0$). Utilizing the fact that

$$N = [2/(2\pi)^3] V_k,$$

we find

$$N_i = \beta_1^i E_i^{3/2} \left[1 + \beta_2^i \left(\frac{E_i}{\delta_0} + \beta_3^i \right)^{-1} \right]^{-1}, \quad (\text{B8})$$

where $i=l$ or h and the β 's are defined as follows:

$$\beta_1^i = (3\pi^2)^{-1} (A \pm \alpha)^{-3/2},$$

$$\beta_2^i = \mp \frac{3}{2} B/\alpha,$$

$$\beta_3^i = (A \pm B)/\alpha,$$

and the upper signs correspond to the case $i=l$.

The density of states is now found from $\mathfrak{D}_i(E)$

$= dN_i/dE_i$, yielding

$$\mathfrak{D}_i(E) = \frac{A_i \Delta_E^2 + B_i \Delta_E + C_i}{(D_i + F_i \Delta_E)^2}, \quad (\text{B9})$$

where $\Delta_E = 2\delta_0$:

$$A_i = \frac{3}{8} (\beta_3^i + \beta_2^i) \beta_1^i \beta_3^i E_i^{1/2},$$

$$B_i = \frac{1}{2} \left(\frac{5}{2} \beta_1^i \beta_2^i + 3 \beta_1^i \beta_3^i \right) E_i^{3/2},$$

$$C_i = \frac{3}{2} \beta_1^i E_i^{5/2},$$

$$D_i = E_i,$$

$$F_i = \frac{1}{2} (\beta_3^i + \beta_2^i).$$

The results for $\vec{\chi} \parallel [111]$ are obtained by making the following substitutions in the above work: $\delta_0 \rightarrow \delta_1 = (d S_{44} / 2 \sqrt{3}) \chi$ and $B \rightarrow \frac{1}{3} N$.

*This work was supported by the National Science Foundation (MRL Program No. GH33574 A-1).

¹J. J. Hall, Phys. Rev. **128**, 68 (1962).

²R. A. Metzler and W. M. Becker, Solid State Commun. **12**, 1209 (1973).

³W. Jakowetz, W. Rühle, K. Breuninger, and M. Pilkuhn, Phys. Status Solidi **12**, 169 (1972).

⁴G. E. Pikus and G. L. Bir, Fiz. Tverd. Tela **1**, 1642 (1959) [Sov. Phys.-Solid State **1**, 1502 (1959)].

⁵M. Cuevas and H. Fritzsche, Phys. Rev. **137**, A1847 (1965).

⁶D. G. Seiler, Ph.D. thesis (Purdue University, 1969) (unpublished).

⁷A. S. Saidov, V. M. Tuchkevich, and Yu. V. Shmartsev, Fiz. Tekh. Poluprovodn. **2**, 891 (1968) [Sov. Phys.-Semicond. **2**, 743 (1968)].

⁸C. F. Lavine and A. W. Ewald, J. Phys. Chem. Solids **32**, 1121 (1970).

⁹C. H. Champness, Phys. Rev. Lett. **1**, 439 (1958).

¹⁰R. J. Stirn and W. M. Becker, Phys. Rev. **148**, 907 (1966).

¹¹B. Lax and J. G. Mavroides, Phys. Rev. **107**, 1530 (1957).

¹²R. A. Stradling, Phys. Lett. **20**, 217 (1966).

¹³M. Reine, R. L. Aggarwal, and B. Lax, Phys. Rev. B **5**, 3033 (1972).

¹⁴A correct theory would require consideration of both optical and acoustic mode scattering, and ionized-impurity scattering, and their energy dependence for each band. The assumption is usually made [see D. M. Brown and R. Bray, Phys. Rev. **127**, 1593 (1962)] that both holes have the same lattice relaxation times. Stirn and Becker [Ref. 10], in a discussion of their magnetoresistance results on p -AlSb using the Champness analysis, point out that the ratio of μ_l/μ_h found experimentally is appreciably lower than expected when

only lattice scattering is considered. They ascribe this result to the neglect of scattering contributions from ionized impurities. Since the light holes are more effectively scattered by ionized impurities than the heavy holes, the light- to heavy-hole mobility ratio should fall below the values expected for lattice scattering alone. In contrast to the results obtained in p -AlSb, values for μ_l/μ_h given in Table I for our p -GaSb samples are not significantly lower than expected for lattice scattering. The application of the Champness analysis does not take into account the theoretical prediction of and experimental evidence for warping of the energy surfaces. This complication is treated later in the text.

¹⁵A. C. Beer and R. K. Willardson, Phys. Rev. **110**, 1286 (1958).

¹⁶A. C. Beer, in *Solid State Physics*, Suppl. 4, edited by F. Seitz and D. Turnbull (Academic, New York, 1963), p. 195.

¹⁷G. L. Bir, E. I. Butikov, and G. E. Pikus, J. Phys. Chem. Solids **24**, 1467 (1963).

¹⁸G. L. Bir and G. E. Pikus, Fiz. Tverd. Tela **3**, 3050 (1961) [Sov. Phys.-Solid State **3**, 2221 (1962)].

¹⁹J. C. Hensel and G. Feher, Phys. Rev. **129**, 1041 (1963).

²⁰E. Kartheuser and S. Rodriguez, Phys. Rev. B **8**, 1556 (1973).

²¹P. Fisher and H. Y. Fan, Phys. Rev. Lett. **5**, 195 (1960); R. L. Jones and P. Fisher, J. Phys. Chem. Solids **26**, 1125 (1965); R. L. Jones, Ph.D. thesis (Purdue University, 1968) (unpublished); S. Rodriguez, P. Fisher, and F. Barra, Phys. Rev. B **5**, 2219 (1972); F. Barra, P. Fisher, and S. Rodriguez, Phys. Rev. B **7**, 5285 (1973).

²²B. J. Roman and A. W. Ewald, Phys. Rev. B **5**, 3914 (1972).

²³A typographical error appearing in Eq. (A3) of Ref. 19 is the omission of δ_0 in the last term under the radical.